than could be accounted for in the various effluents. Unit 3 has the greatest mercury influx, and on a per megawatt basis receives 3½ to 2½ times more mercury than units 7 and 8, respectively. Only 40 to 60 percent of the incoming mercury was accounted for in releases to the atmosphere, with the cooling tower exhaust air being the dominant pathway. Reinjection of excess condensate (cooling tower water) into the geothermal reservoir removed only 0.05 to 0.1 g of mercury per hour. The mercury imbalance at The Geysers could very well be accounted for in the sludge that deposits in the bottom of the cooling towers and must be periodically disposed of in certified landfills. This sludge, which is composed primarily of sulfur from the oxidation of H_2S, contains 0.02 to 0.2 percent mercury. It is difficult to obtain quantitative estimates of the rate of formation of the sludge, but this appears to be an important scavenging mechanism for mercury at The Geysers.

It is of interest to compare the mercury emissions from geothermal power plants with those from coal-fired power plants. Billings *et al.* (*19*) report that a 700-Mwe coal-fired unit releases about 2.3 kg of mercury to the atmosphere each day. On a per megawatt basis this amounts to 3.3 g Mwe^{-1} day^{-1}. At two other coal-fired power plants much lower atmospheric mercury emissions of approximately 0.50 and 0.48 g Mwe^{-1} day^{-1}, respectively, were reported (*20, 21*). Atmospheric mercury emissions from the Cerro Prieto geothermal power plant and from The Geysers units 3, 7, and 8 amounted to 2.2, 1.6, 0.70, and 0.66 g Mwe^{-1} day^{-1}, respectively. Thus, on a per megawatt (electric) basis, the atmospheric releases of mercury from geothermal power plants are roughly comparable to those from coal-fired power plants.

At present there are no Environmental Protection Agency (EPA) mercury emission standards for energy generating facilities. However, the EPA has set a national emission standard for mercury smelters and chlor-alkali plants, which is that the mercury emissions are not to exceed 2300 g released to the atmosphere per 24-hour period (*22*). The atmospheric mercury emissions from 25- to 75-Mwe geothermal power plants (36 to 144 g/day) are far below this standard.

D. E. Robertson
E. A. Crecelius
J. S. Fruchter
J. D. Ludwick

Battelle, Pacific Northwest Laboratories, Richland, Washington 99352

References and Notes

1. S. M. Siegel and B. Z. Siegel, *Environ. Sci. Technol.* **9**, 473 (1975).
2. B. G. Weissberg and M. G. R. Zobel, *Bull. Environ. Contam. Toxicol.* **9**, 148 (1973).
3. A. Eshelman, S. M. Siegel, B. S. Siegel, *Nature (London)* **223**, 471 (1971).
4. R. C. Axtmann, *Science* **187**, 795 (1975).
5. D. E. White, in *Geochemistry of Hydrothermal Ore Deposits*, H. L. Barnes, Ed. (Holt, Rinehart & Winston, New York, 1967), p. 575.
6. ——, M. E. Hinkle, I. Barnes, *U.S. Geol. Surv. Prof. Pap. 713* (1970), pp. 25–28.
7. I. Barnes *et al.*, *U.S. Geol. Surv. Bull. 1382-A* (1973).
8. I. R. Jonasson and R. W. Boyle, *Can. Min. Metall. Bull.* (January 1972), pp. 32–39.
9. J. Olafsson, *Nature (London)* **225**, 138 (1975).
10. R. A. Carr, M. M. Jones, E. R. Russ, *ibid.* **251**, 489 (1974).
11. D. E. Robertson, *BNWL-1950* (Battelle, Pacific Northwest Laboratories, Richland, Wash., 1974), part 2, UC-48.
12. —— and E. F. Briggs, *BNWL-2000* (Battelle, Pacific Northwest Laboratories, Richland, Wash., 1976), part 2, UC-11.
13. K. Boström and D. E. Fisher, *Geochim. Cosmochim. Acta* **33**, 743 (1969).
14. R. G. Yates and L. S. Hilpert, *Calif. J. Mines Geol.* **42**, 231 (1946); E. H. Bailey, *ibid.*, p. 199; C. P. Ross, *U.S. Geol. Surv. Bull. 922-L* (1940), p. 327.
15. D. E. White, L. J. P. Muffler, A. H. Truesdell, *Econ. Geol.* **66**, 75 (1971).
16. M. H. Bothner and D. E. Robertson, *Anal. Chem.* **47**, 592 (1975).
17. R. S. Braman and D. L. Johnson, *Environ. Sci. Technol.* **12**, 996 (1974).
18. J. D. Hem, *U.S. Geol. Surv. Prof. Pap. 713* (1970), pp. 19–23.
19. C. E. Billings, A. M. Sacco, W. R. Matson, R. M. Griffin, W. R. Coniglio, R. A. Harley, *J. Air. Pollut. Control Assoc.* **23**, 773 (1973).
20. G. W. Kalb, in *Trace Elements in Fuel*, S. P. Babu, Ed. (American Chemical Society, Washington, D.C., 1975), p. 175.
21. N. E. Bolton, J. A. Carter, J. F. Emery, C. Feldman, W. Fulkerson, L. D. Hulett, W. S. Lyon, in *ibid.*, p. 175.
22. Anonymous, *J. Air Pollut. Control Assoc.* **23**, 398 (1973).
23. We express our appreciation to the Pacific Gas and Electric Company, Union Oil Company of California, and the Comision Federal de Electricidad of Mexico for granting permission to conduct these studies. In particular, we are indebted to C. Weinberg, G. Sharp, and R. Suess of PG&E and to W. Smith, V. Suter, O. Whitescarver, and R. Pardini of Union Oil for helpful discussions and assistance with fieldwork at The Geysers; to Alfredo Mañon M. and Bernardo Dominguez Aguirre of the Comision Federal de Electricidad for helpful discussions and assistance with fieldwork at Cerro Prieto; and to the Comision's impeccable secretaries. We acknowledge the capable laboratory assistance of E. Briggs, S. Garcia, D. Cochran, and R. Sanders of Battelle, Pacific Northwest Laboratories. We are also grateful to R. Perhac, now at the Electric Power Research Institute, for helpful discussions and guidance during the initial formulation of this program. The work is supported by grant 75-14714 from the National Science Foundation–Research Applied to National Needs.

2 November 1976; revised 13 December 1976

Stable Semiconductor Liquid Junction Cell with 9 Percent Solar-to-Electrical Conversion Efficiency

Abstract. *The semiconductor liquid junction cell* n-*GaAs/0.8*M *K_2Se-0.1*M *K_2Se_2-1*M *KOH/C has been shown to attain 9 percent photovoltaic power conversion efficiency in sunlight. Accelerated tests under 3100°K light sources of several solar intensities indicate very low photocorrosion currents and high output stability.*

We describe the stable operation of a semiconductor liquid junction solar cell which converts solar to electrical power at 9 percent efficiency. The cell consists of an *n*-type GaAs electrode, a carbon counterelectrode, and an aqueous solution of the Se^{2-}/Se_2^{2-} redox couple. The electron-hole pair generated on illumination of the semiconductor is separated by the field near the solution interface (*1*), with the hole moving toward the solution and the electron moving through the bulk of the semiconductor and then through an external load to the counterelectrode. As a result, the illuminated electrode becomes an anode and the counterelectrode a cathode. In a well-behaved cell the oxidation and reduction processes at the two electrodes balance, producing no net chemical change in the solution.

Central to the realization of the concept of these cells is the demonstration of efficient conversion of light to electrical power and of stable operation.

Semiconductor liquid junction solar cells that are based on the *n*-type cadmium chalcogenides CdS (*1–4*), CdSe (*3, 5, 6*), and CdTe (*7*) in the redox electrolytes S^{2-}/S_2^{2-}, Se^{2-}/Se_2^{2-}, and Te^{2-}/Te_2^{2-} have been reported. With several of these combinations, oxidative photoetching of the semiconductor surface under illumination is substantially eliminated (*3, 4, 6, 7*). We have found that the cell CdSe/1*M* Na_2S-1*M* S-1*M* NaOH/C shows an efficiency of 7 to 8 percent for energy conversion at an insolation of ~ 75 mw cm^{-2} (*8*), but this level drops on extended irradiation under load in spite of the apparently minimal evidence of photoetching. We find that the solar cell *n*-CdTe/0.8*M* K_2Se-0.1*M* K_2Se_2-1*M* KOH/C also attains an efficiency near 8 percent. In this case the semiconductor photoetches concurrently at a low rate, but at one sufficient to seriously limit practical life.

We now report that the single-crystal *n*-GaAs/0.8*M* K_2Se-0.1*M* K_2Se_2-1*M* KOH/C solar cell has the highest efficiency so far observed by us (9.0 ± 0.5 percent at an insolation near 70 mw cm^{-2}), yet is sufficiently stable with respect to both photoetching and power output to suggest an effective life of several years. The band gap of GaAs (1.42 ev) is very near the optimum for photo-

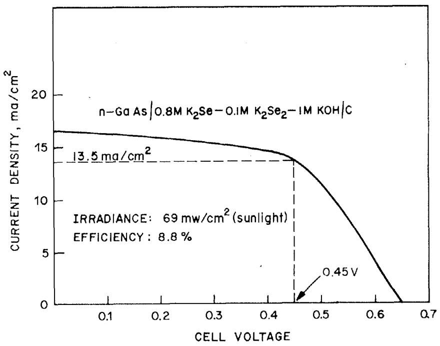

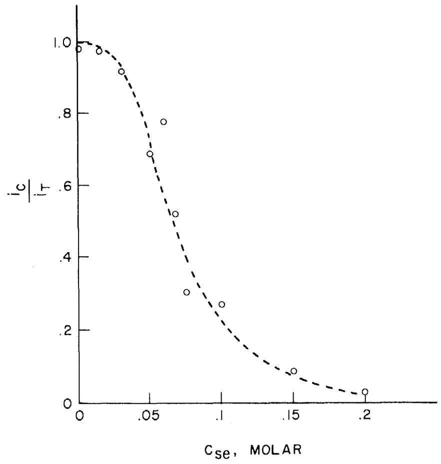

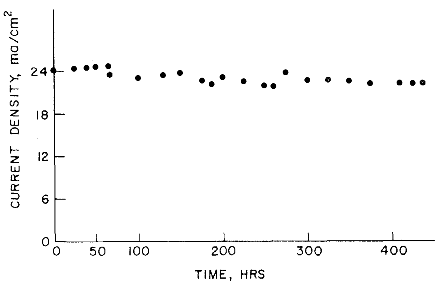

Fig. 1 (left). Current-voltage curve of *n*-GaAs/0.8*M* K_2Se-0.1*M* K_2Se_2-1*M* KOH/C under 69-mw cm^{-2} sunlight. Fig. 2 (top right). Ratio of the corrosion current, i_C, to the total current, i_T, as a function of total selenide concentration, C_{Se}, for *n*-GaAs in 1*M* KOH. Data from electrode weight loss were converted to current at 6 faradays per gram molecule of GaAs. Light intensity was ~ 3 AM2 equivalent from a quartz-halogen lamp. The electrode was potentiostatted at −0.4 volt against a standard calomel electrode. Fig. 3 (bottom right). Current output of *n*-GaAs/0.8*M* K_2Se-0.1*M* K_2Se_2-1*M* KOH/C cell plotted against time under a 50-ohm load and quartz-halogen lamp illumination. The area of the photoanode is 0.35 cm^2. The ordinate values × 17.5 equal cell output in millivolts.

voltaic solar-to-electrical conversion, absorbing light up to about 880 nm.

The current-voltage curve of a typical cell under sunlight is shown in Fig. 1. The short-circuit current at 69 mw cm^{-2} is 16.5 ma cm^{-2}, corresponding to a quantum efficiency of ~ 65 percent if a solar air mass 2 (AM2) spectrum is assumed (*9*). The open-circuit voltage is 0.65 volt. Maximum power is delivered at 0.45 volt and 13.5 ma cm^{-2}, yielding a fill factor of 0.45 × 13.5/0.65 × 16.5 or 57 percent. These data were obtained for a Si-doped specimen with free electron concentration ~ 2 × 10^{17} cm^{-3}, mobility ~ 4000 cm^2 $volt^{-1}$ sec^{-1}, and the previously polished and etched (111) arsenic face exposed to the electrolyte. Similar results were obtained for Sn-doped samples with carrier concentrations near 2 × 10^{17} cm^{-3}, mobilities near 4100 cm^2 $volt^{-1}$ sec^{-1}, and (100) faces. The areas in contact with the solution ranged from 0.1 to 0.3 cm^2.

Many runs with these cells show, for an insolation of ~ 75 mw cm^{-2}, a range of current densities from 14 to 18 ma cm^{-2}, open-circuit potentials from 0.65 to 0.75 volt, and fill factors of 0.55 to 0.72. The product of these factors thus ranges from a minimum of 5.0 to a maximum of 9.7 mw cm^{-2}. For the cell represented in Fig. 1 the product is 6.7 mw cm^{-2}, leading us to anticipate a higher efficiency with better control of the experimental parameters.

At low selenide concentrations illuminated *n*-GaAs undergoes rapid photoetching. At high selenide concentrations photoetching is markedly reduced. This effect is shown in Fig. 2. In the absence of selenide in 1*M* KOH, the etch rate, i_C, confirms the dissolution stoichiometry of six electrons per GaAs molecule found by Harvey (*10*). This factor was used to convert weight loss to current. The ordinate in Fig. 2 is the etch rate divided by the total average current, i_T, and represents the fraction of photocurrent not going to the desired regenerative solar cell path and thus causing etching. The curve drawn in Fig. 2 is a fit to the expression $i_C/i_T = (1 + 3500\,C_{Se}{}^3)^{-1}$, where C_{Se} is the total molar concentration of selenium in the solutions. The $Se^{2-}/Se_2{}^{2-}$ ratio is approximately 8 at all concentrations. A slow rate of magnetic stirring was maintained in all runs and an inert atmosphere (here an argon flow) was necessary to prevent oxidation of selenide by air. In the experiments of Fig. 2, illumination was provided by a quartz-halogen lamp operating at a level sufficient to provide a cell short-circuit current of 50 ma cm^{-2}, which corresponds to a current obtained at ~ 3 AM2 suns. The applied potential of the *n*-GaAs electrode was controlled at −0.4 volt against saturated calomel.

An extended run under similar conditions but at C_{Se} = 1*M* and short circuit to a carbon electrode gave an i_C/i_T ratio of 0.0025. When operated continuously for 18 days near the maximum power point (50-ohm load, ~ 22 ma cm^{-2}, the *n*-GaAs electrode gave i_C/i_T = 0.001 and an average corrosion penetration of less than 12 μm. We estimate that, at this rate, it would take 3.5 × 10^4 hours to dissolve 1 mm of the semiconductor and about three times that, or 10^5 hours, at 1 AM2 sun. Since a conservative use estimate for such a cell would be 3 × 10^3 hour $year^{-1}$, failure by photoetching of a 100-μm layer would not be likely for a period of 3 to 4 years, and even this photoetching rate might be further reduced by increasing the selenide ion concentration.

Figure 3 shows the current-voltage stability of the extended run with the 50-ohm load. A current density of 22 ma cm^{-2} and a voltage of 0.38 were approximately maintained throughout the 432-hour experiment. The slow variation is insufficiently defined to estimate an operating life. We suggest that the output stability derives from the extremely slow but continuous renewal of the surface by semiconductor dissolution. This slow removal process combats performance deterioration by mechanisms involving chemical changes at the semiconductor-liquid junction and in the light-absorbing region near the junction (upper ~ 2 μm). Such changes may include slow ion exchange, adsorption of impurities from solution on the surface of the semiconductor, and diffusion of dopants into the semiconductor depletion layer.

The 9 percent solar-to-electrical conversion efficiency does not match the efficiency of state-of-the-art solid *p-n* junction cells. However, the key to practical cells is in lowering the cost of the power derived. Semiconductor liquid junction cells open avenues to cost reduction by the inherent simplicity of producing the junction and by allowing the use of polycrystalline semiconductors at substantially less sacrifice in efficiency than is encountered in all-solid cells (*11*).

K. C. Chang
A. Heller
B. Schwartz
S. Menezes
B. Miller

Bell Laboratories,
Murray Hill, New Jersey 07974

References

1. H. Gerischer, *J. Electroanal. Chem.* **58**, 236 (1975).
2. _____ and J. Gobrecht, *Ber. Bunsenges. Phys. Chem.* **80**, 327 (1976).
3. A. B. Ellis, S. W. Kaiser, M. S. Wrighton, *J. Am. Chem. Soc.* **98**, 6855 (1976); *ibid.*, p. 1635.
4. B. Miller and A. Heller, *Nature (London)* **262**, 680 (1976).

5. R. A. L. Vanden Berghe, W. P. Gomes, F. Cardon, *Z. Phys. Chem. (Frankfurt am Main)* **92**, 91 (1974).
6. G. Hodes, J. Manassen, D. Cahen, *Nature (London)* **261**, 403 (1976).
7. A. B. Ellis, S. W. Kaiser, M. S. Wrighton, *J. Am. Chem. Soc.* **98**, 6418 (1976).
8. A. Heller, K. C. Chang, B. Miller, *J. Electrochem. Soc.* **124**, 697 (1977).
9. H. J. Hovel, *Semiconductors and Semimetals*, vol. 11, *Solar Cells* (Academic Press, New York, 1975), p. 38.
10. W. W. Harvey, *J. Electrochem. Soc.* **114**, 472 (1967).
11. B. Miller, A. Heller, M. Robbins, S. Menezes, K. C. Chang, J. Thomson Jr., *ibid.*, in press.

10 February 1977; revised 18 March 1977

Clear Air Turbulence: Detection by Infrared Observations of Water Vapor

Abstract. *''Forward-looking'' infrared measurements of water vapor from the C-141A Kuiper Airborne Observatory of the National Aeronautics and Space Administration Ames Research Center show large, distinctly identifiable, signal anomalies from 4 to 10 minutes in advance of subsequent encounters with clear air turbulence (CAT). These anomalies are characteristically different from the signals not followed by CAT encounters. Results of airborne field trials in which the infrared radiometer was used indicate that, out of 51 situations, 80 percent were CAT alerts followed by CAT encounters, 12 percent were ''false alarms'' (CAT alerts not followed by CAT encounters), and 8 percent were CAT encounters not preceded by an infrared signal anomaly or CAT alert.*

The prediction of turbulence at high altitudes (9 to 20 km), especially in clear air, is a problem for both subsonic and supersonic flight. Clear air turbulence (CAT) refers to all forms of turbulence occurring in clear air which do not involve convective forces.

Several investigators have proposed and some have flight-tested infrared (IR) radiometers sensing temperature fluctuations related to CAT in the CO_2 band of the spectrum (*1*, *2*). These techniques have not been totally satisfactory because of a rather high failure rate. Some researchers have suggested that it might also be possible to identify CAT on the basis of water vapor anomalies (*1*). To our knowledge, no one has flight-tested a CAT-sensing radiometer detecting signals in the water vapor bands, at 6.3 μm and at 19.0 to 37.0 μm.

Such a radiometer system has been developed and is flying on the National Aeronautics and Space Administration C-141A Kuiper Airborne Observatory (Fig. 1). The goals are (i) to develop a simple water vapor radiometer system of modest cost that can operate unattended and can achieve accuracy in alerting air crews to CAT encounters from 4.0 to 10.0 minutes before the event and (ii) to study the most probable mechanisms which allow the passive detection of CAT in the water vapor IR bands.

The CAT radiometer employs bandpass filters transmitting from 280 to 520 cm^{-1} or from 1540 to 1670 cm^{-1}. The unit, weighing less than 3.2 kg, is installed ''looking'' forward in the right wheel well of the C-141A heavy jet. The optical system consists of the following components in the order given: a KRS-5 lens, the interference filter, and the detector. A second channel of the same radiometer contains a filter (9.5 to 11.5 μm) to differentiate between clouds ahead and a true water vapor signal anomaly. The radiance arriving at the detector comes from two sources: (i) emission from the water vapor along the column in the field of view of the radiometer and (ii) background emission from clouds or hydrometeors. The radiance (in watts per square centimeter per steradian) may be represented by

$$N = - \int_\nu \int_s B(\nu,T)\, \phi(\nu) \frac{\partial \tau(\mathrm{H_2O})}{\partial s} ds\, d\nu + \int_\nu B(\nu,T_0)\, \phi(\nu)\, \tau_0(\mathrm{H_2O})\, d\nu \qquad (1)$$

where B is the Planck function (in watts per square centimeter per steradian per wave number), ν is the wave number (in reciprocal centimeters), T is the temperature (in degrees Kelvin), ϕ is the filter-detector function, τ is the water vapor transmission, s is the slant path distance (in centimeters), T_0 is the source temperature (in degrees Kelvin), and τ_0 is the total water vapor transmission along the slant path to a source from the detector.

The radiometer is directed upward at a fixed elevation angle of from 2.5° to 7.5°. Inhomogeneities in the water vapor emission entering the 2° cone of acceptance of the radiometer produce anomalies in the detector response and strong signal gradients which are readily detected as sharply varying output signals. After subsequent testing we will also operate the radiometer at elevation angles below the horizontal for anomalies beneath flight level.

Generally, there are two conditions under which CAT may develop. The first is a standing wave in the lee of a mountain barrier which occurs when statically stable air is carried over the mountain. The second condition results from waves formed in statically stable layers in the atmosphere that are subjected to sufficiently strong vertical wind gradients (shear). These shear-induced waves are commonly referred to as Kelvin-Helmholtz (KH) waves. A considerable body of experimental evidence suggests that KH instability is an important mechanism for generating CAT (*3*). When KH waves are of sufficient amplitude, they become unstable and develop into three-dimensional turbulence. Dutton and Panofsky (*4*, p. 944) have stated that ''at least some of the clear air turbulence results from the hydrodynamic instability of internal fronts in accord with the Kelvin-Helmholtz model.''

The onset of KH instability in a statically stable but sheared atmospheric layer is determined by the value of the local Richardson number,

$$Ri = \frac{\dfrac{g}{\theta}\left(\dfrac{\partial\theta}{\partial z}\right)}{\left(\dfrac{\partial U}{\partial z}\right)^2} \qquad (2)$$

Here g is the acceleration of gravity, θ is the potential temperature, z is the height, and U is the horizontal wind velocity. Basically Ri is a measure of the ratio of the potential energy required to overturn a stable layer to the kinetic energy available from the mean shear to accomplish this. A necessary but not sufficient condition for KH instability is expressed by $Ri \leq 0.25$.

Arguments suggest that regions characterized by internal fronts and sloping tropopause are favored areas for KH instability and CAT formations (*5*). These regions, which are statistically linked with the occurrence of CAT, can be identified on the synoptic charts. However, it is virtually impossible to predict in advance when and where individual patches of CAT will occur. Thus, the necessity for an on-board alert system has long been recognized.

It is well known that KH waves ''roll up'' the atmospheric layers in which they form and that the vertical gradients of water vapor in some regions are as much as 20 times greater than their initial undisturbed values. Figure 1 depicts schematically how a transition to KH waves results in the entrainment of water vapor into the breaking waves. As the